Main Manuscript for

A hepatocyte-specific transcriptional program driven by Rela and Stat3 exacerbates experimental colitis in mice by modulating bile synthesis

Jyotsna [1], Binayak Sarkar [1], Mohit Yadav [1], Alvina Deka [2], Manasvini Markandey [5], Priyadarshini Sanyal [3], Perumal Nagarajan [1], Nilesh Gaikward [4], Vineet Ahuja [5], Debasisa Mohanty [1], Soumen Basak [2], Rajesh S Gokhale [1,6]

Affiliation: 1. Immunometabolism Laboratory, National Institute of Immunology, New Delhi 110067;

2. System Immunology Laboratory, National Institute of Immunology, New Delhi 110067;

3. Center for Cellular and Molecular Biology, Hyderabad 500007, Telangana;

4. Gaikwad Steroidomics Lab LLC, Davis, CA 95616;

5. Department of GastroEnterology, All India Institute of Medical Sciences, New Delhi 110067;

6. Department of Biology, Indian Institute of Science Education and Research, Pashan, Pune 411008, Maharashtra;

Corresponding author: Rajesh S. Gokhale.

Email: rsg.nii.ac.in

Author Contributions: J and RSG conceptualized the project. J, BS, MY, AD, MM developed the methodology. J and BS conducted the formal analysis. J, BS, MY, AD, MM, PS performed the investigation. DM, SB, RSG acquired resources for the study. J, SB, RSG wrote the original draft of the manuscript. J, VA, DM, SB, RSG reviewed and edited the manuscript. J was responsible for visualization. RSG supervised the project.

Competing Interest Statement: The authors declare no competing interest.

Keywords: Rela, Stat3, bile acid, colitis, inflammation.

This PDF file includes:

Main Text
Figures 1 to 6 and S1 to S5
Tables S1 to S7

Abstract

Hepatic factors secreted by the liver promote homeostasis and are pivotal for maintaining the liver-gut axis. Bile acid metabolism is one such example wherein, bile acid synthesis occurs in the liver and its biotransformation happens in the intestine. Dysfunctional interactions between the liver and the intestine stimulate varied pathological outcomes through its bidirectional portal communication. Indeed, aberrant bile acid metabolism has been reported in inflammatory bowel disease (IBD). However, the molecular mechanisms underlying these crosstalks that perpetuate intestinal permeability and inflammation remain obscure. Here, we identify a novel hepatic gene program regulated by Rela and Stat3 that accentuates the inflammation in an acute experimental colitis model. Hepatocyte-specific ablation of Rela and Stat3 reduces the levels of primary bile acids in both the liver and the gut and shows a restricted colitogenic phenotype. On supplementation of chenodeoxycholic acid (CDCA), knock-out mice exhibit enhanced colitis-induced alterations. This study provides persuasive evidence for the development of multi-organ strategies for treating IBD and identifies a hepatocyte-specific *rela-stat3* network as a promising therapeutic target.

Main Text

Introduction

Under physiological conditions, the liver is continuously exposed to gut-derived antigens, which are either derived from the food we consume or are the product of microbial metabolism [1]. The continuous interaction of extraneous antigens with the liver tissue makes it a tolerogenic organ, thereby justifying its unique anatomical location [2]. However, during intestinal inflammation or dysbiosis, as seen in conditions like inflammatory bowel disease (IBD), there is an unregulated exchange of molecules across the gut vascular barrier, this potentially rewires the local as well as hepatic immunological and metabolic milieu [3,4]. Over the last decade, several studies have focussed on analyzing the mechanistic aspects of gut-liver crosstalk, which intend to develop successful multi-organ therapies [5,6].

Clinically, IBD overlaps with hepatobiliary conditions, it has been reported that 30% of IBD cases have abnormal liver function tests and around 5% of them even develop chronic hepatobiliary diseases [7, 8]. During colitis, the first responders to extraneous agents incoming from the leaky gut are the Kupffer cells [9]. These cells have been shown to switch from a pro to an anti-inflammatory state in response to signals received from the colitogenic gut [10]. Besides kuffer cells, the parenchymal cells, hepatocytes which occupy ~80% of the liver, also respond to these varied danger signals. Hepatocytes have a robust secretary machinery and are known to secrete a variety of factors like the complement proteins, clotting factors, hepatokines, bile acids etc.

which regulate local as well as distant organ functions [11, 12]. Among the secreted factors, albumin is the most abundantly produced serum protein, which is implicated in the maintenance of redox balance and is known to attenuate DSS-induced colitis [13]. Highlighting the importance of liver secretome, a recent study suggests that FNDC4 has the potential to reduce colonic inflammation by acting on the colonic macrophages [14]. Similarly, bile acids are also known to play a pivotal role in regulating mucosal immune responses. Primary bile acids produced by the liver are often related to an enhanced proinflammatory state and its turnover to secondary bile acids is considered to be a critical step in the maintenance of homeostasis [15]. The primary bile acids have been reported to accumulate in the inflamed colon, suggesting some intriguing crosstalk between the gut and liver [16]. However, it is obscure, how the liver perceives signals due to the disease-mediated impaired gut barrier to rewire secretory machinery and tackle the enhanced endotoxins influx.

Through this study, we propose Rela and Stat3 as key responders of inflammatory signaling in the liver tissue in response to intestinal aberrations. We further define a colitis resistance model based on the liver-specific knockout animals and propose a Rela/Stat3-CYP enzyme-mediated elevation of primary bile acid leading to immune-mediated damage to the gut. Briefly, this study establishes the functional significance of hepatic Rela and Stat3 in intestinal inflammation and emphasises the therapeutic importance of targeting multiorgan crosstalk in inflammatory diseases.

Results

Engagement of hepatic Rela and/or Stat3 pathways in murine colitis model

Several studies have shown that the gut-liver bidirectional communication is critical in both the establishment and progression of IBD. Towards identifying liver pathways that affect intestinal impairment during IBD, we firstly examined whether 2% dextran sodium sulphate (DSS)-induced acute experimental colitis results in changes in liver pathophysiology. Analysis of biochemical parameters on day 6 of DSS treatment showed no significant alterations in the levels of alanine aminotransferase (ALT), aspartate aminotransferase (AST), gamma-glutamyl transferase (GGT) and bilirubin (Figure S1a). Further, histological studies of these treated liver tissues from C57BL/6 mice showed neither morphological differences nor any hepatocellular fibrosis (Figure S1b). Thus, in general, the liver functionalities are maintained and no major damage in the liver tissue occurs in the colitogenic mice model. We then performed global transcriptomic studies of the liver tissue from day 6 colitogenic mice. Unsupervised clustering of the transcriptome data by principal component analysis (PCA) segregated the treated and control

samples on PC1 with a variance of 53% (Figure S1c). Immunological and metabolic pathways appeared to be enriched in the list of regulated pathways. LPS-mediated signaling in the liver was identified as among the key differentially expressed systems (Figure 1A). It is proposed that microbial components, including LPS from the gut, can reach the liver through portal blood, activating the hepatic immune response during colitis-mediated barrier impairment. Interestingly, Rela and Stat3 are two important transcription factors activated by the microbial LPS and these two pathways frequently converge to elicit protective responses [17, 18, 19, 20]. Further analysis of transcript abundance of Rela, Stat3, and other downstream genes reflected higher transcript abundance in the DSS-treated group as compared to the control (Figure 1B). Functional activation of Rela and Stat3 pathways requires phosphorylation of key residues, which we investigated in the liver sections of DSS-treated mice. Immunostaining studies showed an enhanced signal intensity of p-Rela (Ser536), p-Stat3 (Ser727) and p-Stat3 (Tyr705) in the treated liver sections, as compared to untreated samples (Figure 1C).

We then examined time-dependent phosphorylation status of the two proteins of the liver post 0, 2, 4, and 6 days of DSS treatment. The RelA phosphorylation at Ser536 peaks at day 2 (about eight fold increase) following which a two to three fold increase was sustained till day 6 (Figure 1D and E). The Stat3 phosphorylation at Ser727 increases gradually from day 2 (eight-fold) to day 6 (seventeen-fold). Tyrosine phosphorylation on the other hand, is transient and can be detected at day 4 (nine-fold) post-treatment (Figure 1D and E).

Antibiotic-induced gut microbiome depletion has been frequently used to study gut microbiome roles in pathological conditions. Altered microbiota is also likely to modulate endotoxin influx. We therefore examined hepatic Rela/Stat3 activation after subjecting mice to oral administration of a broad-spectrum antibiotic cocktail (Amplicin, Neomycin, Metronidazole and Vancomycin) [21]. Substantial decrease in bacterial load after four weeks was confirmed microbiologically. We induced colitis in mice with 2% DSS treatment along with antibiotic administration (Figure S1d and Supplementary methods). Previous data indicates that pStat3 (Ser727) is the most prominent marker that gets highly activated 6 days post DSS-treatment. Time course activation studies had indicated pStat3 (Ser727) as the most prominent marker to be activated six days post DSS-treatment; we examined the levels through western blotting. A marked reduction in pStat3 (Ser727) levels post-antibiotic treatment in the colitogenic wild type mice (Figure S1e) could be noted, suggesting that optimal endotoxin flux may be a major driver of hepatic Rela/Stat3 signalling. Although it is important to note that antibiotic-induced microbiome depletion alters metabolic homeostasis by affecting gut signaling and colonic metabolism, in turn altering hepatic physiology [22].

Hepatocyte-specific functions of Rela and Stat3 exacerbate experimental colitis

In order to discern the importance of transcriptional networks regulated by Rela and Stat3 we utilized a hepatocyte-specific knockout model. The Cre recombinase under albumin promoter drives the deletion of Rela and/or Stat3 in a tissue-specific manner (Figure S2a and S2b). To address the question, if ablation of Rela and Stat3 functioning in hepatocytes could modulate colonic inflammation, we subjected *rela*$^{\Delta hep}$, *stat3*$^{\Delta hep}$, *rela*$^{\Delta hep}$*stat3*$^{\Delta hep}$ and wild type littermates mice to acute DSS treatment. Previous studies suggest development of colitis in acute models is accompanied by shortening of the colon length, diarrhea and rectal bleeding which is measured as the disease activity index (DAI) [23]. Time course measurement of DAI in the wild type showed expected increase from day three (Figure 2A). While the DAI in *rela*$^{\Delta hep}$ mice was parallel to that observed in wild type mice, *stat3*$^{\Delta hep}$ mice displayed a subtle decrease in the DAI score, particularly on day five. Surprisingly, *rela*$^{\Delta hep}$*stat3*$^{\Delta hep}$ mice were almost resistant to induction of colitis, and only a minor increase in the DAI could be seen on day 6 post-onset of DSS treatment (Figure 2A). Concurrently, DSS treatment for six days showed substantial shortening of the colon length in wild type, *rela*$^{\Delta hep}$, and *stat3*$^{\Delta hep}$ mice, but not in *rela*$^{\Delta hep}$*stat3*$^{\Delta hep}$ mice (Figure 2B and S2c). Further, we estimated the intestinal barrier permeability by measuring serum concentrations of fluorescein isothiocyanate (FITC)-dextran which was gavaged orally to these mice. A twelve fold increase in FITC-dextran in the serum of the wild type animals was seen, while the *rela*$^{\Delta hep}$*stat3*$^{\Delta hep}$ mice showed substantially lower, five-fold increase (Figure 2D).

We also examined *rela*$^{\Delta hep}$*stat3*$^{\Delta hep}$ mice for the epithelial architecture and mucin expression in colon by following histological features and expression of colitogenic markers. DSS treatment led to extensive disruption of the intestinal crypts and depletion of the mucin layer in wild type mice, accompanied by submucosal leukocyte infiltration. In contrast, *rela*$^{\Delta hep}$*stat3*$^{\Delta hep}$ mice showed substantially attenuated epithelial changes along with minimal erosion of mucin layers (Figure 2C and S2d). RT-qPCR analysis revealed that DSS treatment of wild type mice triggered a two and a half-fold and two-fold reduction in the colonic abundance of enterocyte markers, tight junction 1 (tjp1) and occludin (ocln), respectively (Figure 2E). Similarly, we noticed a four-fold and two-fold decrease in the colonic abundance of goblet cell markers, mucins-2 and trefoil factor 3 (tff3), respectively, in wild type mice upon DSS treatment. Except for a moderate decrease in the Tjp1 mRNA level, none of these mRNAs were downregulated upon DSS treatment in *rela*$^{\Delta hep}$*stat3*$^{\Delta hep}$ mice. Taken together these studies reveal intriguing observations wherein the absence of Rela and Stat3 in hepatocytes protects mice from DSS-induced colitis.

Induced hepatic expression of Rela and Stat3 stimulates primary bile acid synthesis pathway genes.

To understand the role of the liver in imparting protective phenotype, exhibited by *rela*$^{\Delta hep}$*stat3*$^{\Delta hep}$ strain, we performed an in-depth pathophysiological and molecular studies of the liver tissue of colitogenic knockout animals. Towards this, we evaluated the serum-based liver damage markers and histological features of the *rela*$^{\Delta hep}$*stat3*$^{\Delta hep}$ mice. On day 4 and day 6 post DSS-treatment, ALT, AST, GGT and bilirubin levels were within the physiological range, indicating no apparent damage to the liver (Figure S3a). Similarly, the histological studies also suggested no morphological differences in the DSS-treated *rela*$^{\Delta hep}$*stat3*$^{\Delta hep}$ mice (Figure S3b). In conclusion, the above data indicates that the liver functions are maintained in the colitogenic *rela*$^{\Delta hep}$*stat3*$^{\Delta hep}$ mice, similar to that observed in the wild type animals. Further, to dissect the mechanism underlying the resistant phenotype displayed by hepatocyte-specific *rela*$^{\Delta hep}$*stat3*$^{\Delta hep}$ mice, we performed global transcriptome studies from liver tissues of treated/untreated *rela*$^{\Delta hep}$*stat3*$^{\Delta hep}$ strain and their wild type littermates. Unsupervised clustering of transcriptomic data using PCA tool segregate wild type and *rela*$^{\Delta hep}$*stat3*$^{\Delta hep}$ mice samples subjected to DSS treatment (Figure 3A). Notably, untreated mice from wild type and *rela*$^{\Delta hep}$*stat3*$^{\Delta hep}$ cluster together in the PCA plot. Comparative pathway enrichment analysis using GO terms for differentially expressed genes in the liver upon DSS treatment between wild type and *rela*$^{\Delta hep}$*stat3*$^{\Delta hep}$ mice showed differences in the acute phase responses, bile acid metabolic processes, response to ER stress, and one-carbon metabolism (Figure 3B). BA dysmetabolism has been reported in IBD patients by several studies and is also recapitulated in the mice models [24, 25]. The consensus thesis is that the levels of secondary BAs are lower, primary BAs are elevated because of impairment of microbiota-mediated deconjugation and transformation activities. Concordantly, our analysis from colonic biopsies of IBD subjects also showed elevated levels for primary BAs (Figure 3C).

BAs are synthesized in hepatocytes through the classical and alternate pathways catalyzed by a set of P450 enzymes (Figure 3D). Cholic acid (CA) and chenodeoxycholic acid (CDCA) are primary bile acids and are conjugated to either glycine (predominantly in humans) or taurine (mainly in mice). Transcriptomics data strikingly showed downregulation of Cyp7b1 in the *rela*$^{\Delta hep}$*stat3*$^{\Delta hep}$ mice and the other biosynthesis enzymes also follow a similar trend (Figure S3c-e). Our RT-qPCR analyses substantiated that in comparison to DSS-treated wild type mice, DSS-treated *rela*$^{\Delta hep}$*stat3*$^{\Delta hep}$ mice expressed a reduced level of mRNAs encoding primary bile acid synthesis pathway enzymes Cyp7a1, Cyp8b1, Cyp27a1 and Cyp7b1 in the liver (Figure 3E). Thus, our data propose a new hypothesis that hepatic Rela and Stat3 instruct a gene program in the liver of colitogenic mice that supports the expression of mRNAs encoding primary BA metabolism enzymes.

Reducing the levels of primary bile acids dampened intestinal inflammation in colitogenic *rela$^{\Delta hep}$stat3$^{\Delta hep}$* mice.

To investigate if the altered hepatic gene expression led to a change in the abundance of primary bile metabolites in *rela$^{\Delta hep}$stat3$^{\Delta hep}$* mice, we performed a targeted metabolomic study using LC-MS. Apart from measuring CA and CDCA, we also measured the level of CDCA-derived bile metabolites, namely ursodeoxycholic acid and α- and β-muricholic acid which are specifically produced in mice [26]. Our analyses revealed the abundance of cholic acid in the liver, which was approximately seven-fold less in DSS-treated *rela$^{\Delta hep}$stat3$^{\Delta hep}$* mice compared to their wild type counterparts (Figure 4A). Likewise, we captured a close to ten-fold decrease in the hepatic level of CDCA in DSS-treated knockout mice. A substantially reduced levels of ursodeoxycholic acid and α-muricholic acid. We further compared DSS-treated wild type and *rela$^{\Delta hep}$stat3$^{\Delta hep}$* mice for the colonic abundance of these bile acids. Consistent with the levels observed in the liver, we found a significantly reduced accumulation of both CA and CDCA in the colon of DSS-treated *rela$^{\Delta hep}$stat3$^{\Delta hep}$* mice. The difference between wild type and knockout mice was substantially more marked for CDCA (Fig 4B).

CDCA has been reported to engage the NLRP3 inflammasome, causing liver inflammation during cholestasis [27]. Further, ex vivo experiments have shown that CDCA induces pro-inflammatory cytokine secretion by intestinal epithelial cells [28]. Because we noticed an altered abundance of these primary bile acids in *rela$^{\Delta hep}$stat3$^{\Delta hep}$* mice, we asked if DSS treatment dampened the pro-inflammatory response in these knockouts. Indeed, compared to DSS-treated wild type mice, DSS-treated knockout mice presented with substantially reduced level of mRNAs encoding key pro-inflammatory cytokines, namely Il1b, Tnfa, and Il6 (Fig 4C). Consistent with the less inflamed intestinal milieu, *rela$^{\Delta hep}$stat3$^{\Delta hep}$* mice also displayed a diminished frequency of inflammatory effector immune cells in the colitogenic gut (Fig 4D and S4a). Confocal microscopy-based analyses of stained colon sections depicted a close to five-fold reduction in the recruitment of Ly6G+ cells, including neutrophils and monocytes, F4/80+ macrophages, and CD11c+ including macrophages and the dendritic cells in DSS-treated knockout mice, compared to their wild type counterparts (Figure 4D and S4a). Taken together, we propose that a reduced accumulation of primary bile acids alleviates experimental colitis in *rela$^{\Delta hep}$stat3$^{\Delta hep}$* mice.

Supplementing chenodeoxycholic acid restores colitogenic sensitivity of *rela$^{\Delta hep}$stat3$^{\Delta hep}$* mice.

Recent studies have highlighted the role of CA in potentiating intestinal damage by impairing Lgr5^{+} intestinal stem cells. However, the role of CDCA in regulating intestinal inflammation in colitogenic mice remains unclear. Therefore we supplemented CDCA

intraperitoneally daily for six days during DSS treatment in the wild type or *rela*$^{\Delta hep}$*stat3*$^{\Delta hep}$ mice and scored the DAI (Figure S5a). The optimum concentration of CDCA was determined by performing a dose-response curve. Mere daily supplementation of CDCA at the concentration of 10 mg/kg of body weight, elevated the levels of CDCA in colon (Figure S5b) without inducing any colitogenic phenotype in either wild type or *rela*$^{\Delta hep}$*stat3*$^{\Delta hep}$ mice even after six days (Fig S5 c-e). Moreover, the DAI of wild type mice treated with both DSS and CDCA showed no change (Figure 5A). On the other hand, CDCA supplementation of the DSS-treated *rela*$^{\Delta hep}$*stat3*$^{\Delta hep}$ mice showed DAI equivalent to wild type DSS-treated mice with concomitant supplementation of colon length shortening (Figure 5A and Figure 5B). Histological analyses of DSS-treated colon sections further substantiated that CDCA supplementation together with DSS treatment was sufficient for imparting damage to the colonic crypts of the colitis-resistant *rela*$^{\Delta hep}$*stat3*$^{\Delta hep}$ mice (Figure 5C). Consistent with the observed intestinal pathologies, bile acid supplementation also triggered a drastic reduction in the colonic abundance of mRNAs encoding the junctional proteins Tjp1 and Ocln as well as Muc2 in DSS-treated *rela*$^{\Delta hep}$*stat3*$^{\Delta hep}$ mice (Figure 5D). Concurrently, bile acid-supplemented *rela*$^{\Delta hep}$*stat3*$^{\Delta hep}$ mice show prominently upregulated expression of genes encoding the pro-inflammatory cytokines Il1b, Tnfa and Il6 upon DSS treatment, compared to those treated with DSS alone (Figure 5E). Thus, we conclude that RelA and Stat3-driven accumulation of CDCA aggravates intestinal inflammation-induced damage during experimental colitis.

Discussion

IBD are a heterogeneous group of chronic inflammatory intestinal disorders that are influenced by environmental cues, intestinal dysbiosis and the local immune responses [29, 30]. Chronic intestinal inflammation remodels the permeability barrier resulting in leakage of microbial components, including LPS, through the portal circulation thereby engaging extraintestinal organs such as the liver. The conventional treatment regimen for IBD involves aminosalicylates, corticosteroids and anti-TNF agents to counter bowel inflammation [31]. Systemic effects are only addressed upon worsening of symptoms [32]. To improve the clinical management of IBD, there is a need to identify targets and mechanisms that can concurrently address other associated causes. In this study, we reveal the surprising role of hepatic rela-stat3 in regulating the biosynthesis of primary bile acids, whose activation augments intestinal inflammation.

Lipopolysaccharides (LPS), one of the key components of microbial products, is known to induce inflammasome assembly by NF-κB/Lipocalin2-dependent axis in macrophages of colitogenic mice [33]. Similarly, LPS-mediated non-canonical Stat3 activation through TLR4 ligand reprograms metabolic and inflammatory pathways in macrophages [17]. In the acute DSS-induced colitis model, the release of LPS and other endotoxins would first activate kupffer cells of the liver,

which then progressively triggers a response in relatively quiescent hepatocytes [10]. We argued that Stat3-NF-κB signalling may be of specific significance since these pathways in hepatocytes are known to control the secretion of hepatic factors. We indeed observed activation of the canonical arm of the NF-κB signalling pathway with RelA phosphorylation at Ser536 residue following DSS treatment. Interestingly, non-canonical Stat3 activation was detected with Ser727 phosphorylation preceding the phosphorylation of canonical Tyr705 residue. To understand the significance of these signalling pathways of hepatocytes in the context of disease outcomes and its functional consequence in disease management, we subjected the single and double hepatocyte-specific knockout mice to DSS treatment. Surprisingly, the *rela*$^{\Delta hep}$*stat3*$^{\Delta hep}$ mice had attenuated disease activity index as well as diminished inflammatory response in the gut. Previous studies wherein attenuation of colitogenic phenotype has been reported are for the gut-resident cells [34, 35, 36, 37]. This study is amongst the first such, where ablation of genes in a distal organ - the liver - ameliorates colitis.

We then investigated the mechanisms underlying signalling networks in the liver that promote the colitis phenotype. Previously, hepatic Rela and Stat3 have been reported to act cooperatively to render protection against pulmonary infection, by eliciting an acute phase response, which enhances the pulmonary immune response [38, 39]. We observe similar hepatic functions of Rela and Stat3 that amplify the immune response during experimental colitis, aggravating intestinal pathologies. Our unbiased transcriptome analysis of the liver genes revealed several metabolic and immune pathways to be altered in colitogenic mice. Amongst these, the biosynthesis of primary BAs prompted our immediate attention. The primary bile acids are known to have inflammatory activity and the cardinal paradigm in IBD is the decreased levels of secondary bile acid [40, 41]. This has been attributed to the altered gut microflora that are known to convert primary BAs into secondary BAs. It is important to note that most of these studies are carried out with fecal samples and a recent study that profiled the human intestinal environment under physiological conditions concluded that stool-based measurements do not reflect the true composition of BAs along the intestinal tracts. Intestinal samples were dominated by primary BAs, whereas stool samples were dominated by secondary BAs [42]. We therefore measured the intestinal BAs in IBD subjects by using mucosal biopsies and observed elevated levels of primary BAs in the IBD subjects as compared to non-IBD subjects.

Analysis of colitogenic mice intestinal samples also revealed enhanced primary BAs using mass spectrometry-based measurements. We observe both CDCA and CA accumulate in the intestine and liver of colitogenic wild type mice when compared to knockout littermates. This accumulation of primary BA in both the intestine and liver is likely to be a consequence of increased biosynthesis in the liver and subsequent transport to the gut. Indeed, multiple primary

bile synthesis pathway genes namely cyp7a1, cyp27a1, cyp7b1, and cyp8b1 were substantially upregulated in the liver. Our observation is contradictory to the recently published work by Gui et al which suggests that during IBD there is a downregulation of the biosynthesis machinery leading to reduced bile levels [43]. Currently, we assume that these differences may arise due to the dose of DSS, the time course of the experiment and the mice strain adapted for different studies leading to the difference in the transcriptional and metabolic landscape during IBD [43, 44 ,16] .

Conventionally the cyp450 enzymes involved in the bile acid biosynthesis pathway are known to be regulated by the FXR signaling cascade [45]. Our data suggest that RelA and Stat3 transcriptionally control these pathways under stress conditions. These two transcription factors have been known to collaborate in a variety of physiological and disease settings. Further studies would elucidate a mechanistic understanding of how these hepatocyte-specific transcriptional regulatory circuitry drives hepatic bile synthesis during gastrointestinal abnormalities. Mutant mice showed refractory behavior towards colitogensis, where mere supplementation of CDCA resulted in exacerbated colitis phenotype in the gut. Previous studies of increased CA have been attributed to colitis and CA was shown to limit the self-renewal capacity of intestinal stem cells leading to impaired intestinal restitution [44]. We now propose that increased synthesis and secretion of the primary bile acids orchestrates intestinal inflammation. It is increasingly important to understand how bile acid signaling networks are affected in distinct organs where the bile acid composition differs, and how these networks impact intestinal diseases. Our studies identify a new, important Rela-Stat3 network system of hepatocytes that could enable the development of therapeutics that targets BA imbalance by suppressing host-specific stress-induced pathways.

Until now, only immunosuppressive agents and immunomodulators have been conventionally considered as therapeutic measures to manage IBD. However, with increasing research on the role of hepatic bile acid metabolism during experimental colitis, its potential cannot be undermined in the clinical setting. The potential of bile acids as a therapeutic target has been harnessed in the past; bile acid sequestrants have been utilized as a treatment for hyperlipidemia [46]. Remedies like fecal microbial transplantation, which serve to normalize the bile acid ratios in the gut, are emerging as potential therapeutics in the last decade for IBD [47, 40]. However, the potential of altering hepatic bile metabolism has remained unexplored for IBD, possibly due to a lack of mechanistic insight. Towards this, our work demonstrates the pro-inflammatory potential of CDCA during colitis following the activation of the Rela/Stat3 pathway. The suppression of Rela/Stat3-induced CDCA could provide beneficial effects in IBD patients while protecting the basal bile acid levels (through FXR signaling). Thus our studies identify a hepatocyte-specific rela/stat3 network as a potential therapeutic target for intestinal

diseases. Another approach could be the use of bile acid sequestrants, which will temporarily decrease the levels of primary bile acids in the colon until the proinflammatory pathways are dampened as a combinatorial therapy alongside existing treatments.

Materials and Methods

Human Studies

All studies were approved by the All India Institute of Medical Science Ethics Committee for postgraduate research (Approval number – IECPG-270/22.04.2019). Biopsy specimens were collected from recto-sigmoidal or sigmoidal colon regions. Ulcerative colitis patients with mild-to-moderate disease activity (SCCAI: 3-9) were included in the IBD group. Subjects undergoing sigmoidoscopy for inspection of manifestations such as haemorrhoidal bleeds were included in the non-IBD group. Patients with severe disease activity, history of antibiotics or topical steroids in the past 4 weeks, pregnancy, comorbid illnesses and/or history of bowel surgery were excluded. These samples were immediately stored at -80 degrees Celsius in cryovials till further processing.

Animal Studies

All mouse strains were housed at the National Institute of Immunology (NII) and utilized adhering to the institutional guidelines (Approval number – IAEC 579/21). 5-7 week old C57BL/6 mice were used. Hepatocyte-specific knockout animals (Cre under albumin promoter) *rela*$^{\Delta hep}$, *stat3*$^{\Delta hep}$ and *rela*$^{\Delta hep}$*stat3*$^{\Delta hep}$ along with their Cre-negative (referred to as wild type in the text) littermates *rela*$^{fl/fl}$, *stat3*$^{fl/fl}$, and *rela*$^{fl/fl}$*stat3*$^{fl/fl}$ were generously gifted by Dr. Lee Quinton, School of Medicine, Boston University, Boston, MA, USA. Above mentioned knockout strains were crossed with their corresponding wild type littermates to expand the colonies for experimental purposes at the small animal facility.

Induction and assessment of colitis in mice

As described earlier [48], 5-7 weeks old male/female (18-21 g body weight) mice of the indicated genotypes were randomly chosen for administered with 2% of DSS in drinking water for six days. Subsequently, body weight and disease activity were assessed for six days from the onset of DSS treatment. All experiments were performed using littermate mice cohoused for a week prior to the initiation of the experiments. The disease activity index was estimated based on stool consistency and rectal bleeding. The score was assigned as follows – 0 points were given for well-formed pellets, 1 point for pasty and semi-formed stool, 2 points for liquid stool, 3 points for bloody smear along with stool, and 4 points were assigned for bloody fluid/mortality. Mice with

more than 30% loss of body weight were considered moribund, and euthanized. For specific experiments, mice were euthanized at the indicated days post-onset of DSS treatment, and colon tissues were collected.

10 mg/kg body weight of chenodeoxycholic acid dissolved in DMSO was injected via intraperitoneal route into mice as described earlier [49].

Histopathological studies

At day six of DSS treatment, mice with the indicated genotypes were euthanized, and the entire colon was excised. The colon length was measured from the rectum to the caecum. Subsequently, distal colons were washed with PBS, fixed in 10% formalin, and embedded in paraffin. 5µm thick tissue sections were generated from the inflamed region and stained with hematoxylin and eosin (H&E). Alternately, sections were stained with Alcian Blue for revealing mucin content. Images were acquired using Image-Pro6 software on an Olympus inverted microscope under a 20X objective lens. The severity of colitis was assessed by epithelial damage and infiltration of inflammatory immune cells in the submucosa of the colon.

For assessing intestinal permeability, FITC-dextran was orally gavaged to untreated or DSS-treated mice 6 hours prior to sera collection. Fluorescent based quantitation of sera samples were performed using CLARIOstar microplate reader (λ_{ex} : 490 nm and λ_{em}: 520 nm).

Confocal microscopy: sample preparation & analysis

Sample preparation: Distal colon samples were fixed in 10% formalin for 24 hrs. Fixed sections were embedded in paraffin and 5-µm based sections were generated using microtome. Deparaffinization of sections were achieved by snap heating followed by xylene wash, subsequently, these were rehydrated. Antigen retrieval was performed using a sodium citrate buffer (10mM, pH 6.0) at 95 degrees for 10 minutes and the slides were allowed to cool down. Further, these were rinsed in PBS, permeabilized for 5 min in 0.4% PBST, and blocked for 1 hour in 5% bovine serum albumin. These sections were stained with fluorescently conjugated antibodies listed in table 1 for overnight at 4 degree. Non-conjugated primary antibodies were incubated O/N at 4 degrees followed by incubation of conjugated secondary antibody for 2hrs. Subsequently, the slides were rinsed in PBS and incubated with DAPI for nuclear staining. Finally, slides were mounted using fluoroshield mounting media, and slides were analyzed under ZEISS LSM 980 confocal microscope at 40X (oil) magnification.

For analysis, the ratio between the signal of interest / DAPI was calculated for every field. Each dot represents the average ratio for 5 individual fields of interest. The plot is representative data

from 3 biological replicates.

Gene expression studies

Total RNA was isolated using MN-NucleoSpin RNA (as per manufacturer's instructions) from the liver and colon of untreated and DSS-treated animals of indicated genotypes. cDNA was synthesized using Takara cDNA synthesis kit as per manufacturer protocol. RT-qPCR was performed using PowerUp SYBR Green PCR master mix in ABI 7500 FAST instrument. Relative mRNA levels were quantitated and GAPDH was used as a control.

Further, RNA isolated from liver tissue was subjected to paired-end RNA-sequencing after rRNA depletion, on Illumina platform 6000 at core facility of the CCMB, India. Twenty million unique RNA fragments were sequenced per sample and the average length of the sequenced reads was around 150bp. The RNA-seq raw data is available in the NIH National Center for Biotechnology Information GEO database as GSE243307. Quality control and sequence trimming was performed using fastp (v0.23.2). The trimmed paired-end reads were aligned to the mouse genomes (mm9) using the HISAT2 (v2.2.1) pipeline. Reads were assembled into transcripts using StringTie (v2.2.1). Annotation was conducted using aligned sequences and a GTF annotation file. The mapped reads were then used for generating the count table using StringTie (v2.2.1). We had a total of 51,610 entries in our dataset for which differential expression analysis was performed using the DEseq2 R package. Pathway enrichment was performed using the GO database and clusters were visualized using the R package ClusterProfiler.

Biochemical studies

Immunoblot analyses:

Tissue fragment (colon or liver) were homogenized in hand held douncer in SDS-RIPA buffer (50 mM Tris-HCl pH 7.5, 150 mM NaCl, 1 mM EDTA, 0.1% SDS, 1% Triton-X 100, 1 mM DTT, 1X Proteinase inhibitor, 1X Protease inhibitor). Subsequently these extracts were centrifuged and the supernatants were resolved by SDS-PAGE and transferred onto a PVDF membrane, and immunoblotting was performed using indicated antibodies. Blots were developed using Immobilon HRP substrate and images were acquired through ImageQuant Chemiluminescent imaging system (LAS 500). Band intensities were quantified in ImageJ.

Targeted Metabolomics:

Lipid pools were extracted by a two-step liquid-liquid extraction protocol as described previously [50]. Specific weight of the murine tissue was homogenized in methanol twice using 1.0 mm

Zirconium beads. Extracted tissue pellets were subjected to chloroform extraction using a bath sonicator twice. The methanol and chloroform fractions were pooled and evaporated using speed-vac. Samples were added with 150ul MeOH, vortexed, sonicated and filtered (0.45 µm) for further analysis. A triple quadruple mass spectrometer (Waters, Milford, MA, USA) recorded MS and MS/MS spectra using electrospray ionization (ESI) in negative ion (NI) mode. Waters Acquity UPLC system was connected to the triple-quadrupole mass spectrometer. Analytical separations of the mixture of specific primary BAs were performed on the UPLC system using an ACQUITY UPLC C18 (1.6 mm 1*150 mm) analytical column.

Untargeted Metabolomics:

5mg of biopsy material was transferred to pre-chilled homogenizer vials, mixed with 80% methanol and subjected to 3 rounds of homogenization, each with 2 cycles of 30sec. The homogenate was centrifuged at 14000 g for 20 min at 4 degrees Celsius and thereafter dried overnight in Speed Vac. At the time of sample run the samples were resuspended in 15% ACN for Reverse Phase Chromatography, and LC/MS was performed on ThermoFisher Orbitrap Fusion Tribrid Mass Spectrometer.

Statistical analysis

Quantified data for 3-6 mice replicates were plotted as mean ± SEM (represented as error bars). Unless otherwise mentioned, unpaired two-tailed Student's t-test and one-way Anova was used for calculating statistical significance in data sets involving two groups and multiple groups respectively.

Acknowledgements

We thank Dr. Lee Quinton for providing us with hepatocyte specific knockout animals for *rela* and/or *stat3* for carrying out this study; Dr. Devram S. Ghorpade, NII, New Delhi for discussions; Next Generation Sequencing (NGS) facility at CSIR-CCMB for the transcriptomic support; Mass Spectrometric facility at THSTI, Faridabad for the metablomic support; the Small Animal Facility at the National Institute of Immunology, New Delhi for support with mice providing the breeding and experimental support; the Department of Biotechnology (DBT) for institutional support provided to National Institute of Immunology.

Data and Material Availability:

The mice strain used have been gifted by Dr. Lee Quinton from Boston University and is available at the breeding facility at the National Institute of Immunology. All materials and reagents will be available on request. The transcriptomic data will be available online at GEO with accession id GSE243307. All codes used for the analysis is publically available and can also be provided upon request.

References

1. Tripathi, A. *et al.* The gut–liver axis and the intersection with the microbiome. *Nat. Rev. Gastroenterol. Hepatol.* **15**, 397–411 (2018).
2. Horst, A. K., Neumann, K., Diehl, L. & Tiegs, G. Modulation of liver tolerance by conventional and nonconventional antigen-presenting cells and regulatory immune cells. *Cell. Mol. Immunol.* **13**, 277–292 (2016).
3. Kobayashi, T., Iwaki, M., Nakajima, A., Nogami, A. & Yoneda, M. Current Research on the Pathogenesis of NAFLD/NASH and the Gut-Liver Axis: Gut Microbiota, Dysbiosis, and Leaky-Gut Syndrome. *Int. J. Mol. Sci.* **23**, (2022).
4. Bailey, M. A. *et al.* Dietary fiber intake and fecal short-chain fatty acid concentrations are associated with lower plasma lipopolysaccharide-binding protein and inflammation. *American Journal of Physiology-Gastrointestinal and Liver Physiology* (2023) doi:10.1152/ajpgi.00176.2021.
5. Tilg, H., Adolph, T. E. & Trauner, M. Gut-liver axis: Pathophysiological concepts and clinical implications. *Cell Metab.* **34**, 1700–1718 (2022).
6. Kessoku, T. *et al.* The Role of Leaky Gut in Nonalcoholic Fatty Liver Disease: A Novel Therapeutic Target. *Int. J. Mol. Sci.* **22**, (2021).
7. Cappello, M. *et al.* Liver Function Test Abnormalities in Patients with Inflammatory Bowel Diseases: A Hospital-based Survey. *Clin. Med. Insights Gastroenterol.* **7**, 25–31 (2014).
8. Gaspar, R., Branco, C. C. & Macedo, G. Liver manifestations and complications in inflammatory bowel disease: A review. *World J. Hepatol.* **13**, 1956–1967 (2021).
9. Yamada, T. *et al.* Kupffer-cell depletion attenuates colonic and extracolonic granulomatous

inflammation in chronic colitis. *J. Lab. Clin. Med.* **142**, 268–277 (2003).

10. Taniki, N. *et al.* Intestinal barrier regulates immune responses in the liver via IL-10-producing macrophages. *JCI Insight* **3**, (2018).
11. Kwon, J., Lee, C., Heo, S., Kim, B. & Hyun, C.-K. DSS-induced colitis is associated with adipose tissue dysfunction and disrupted hepatic lipid metabolism leading to hepatosteatosis and dyslipidemia in mice. *Sci. Rep.* **11**, 5283 (2021).
12. Zhu, L. *et al.* Multi-Omics Analysis of the Gut-Liver Axis Reveals the Mechanism of Liver Injury in Colitis Mice. *Front. Immunol.* **12**, 773070 (2021).
13. Yang, X. *et al.* Reductively modified albumin attenuates DSS-Induced mouse colitis through rebalancing systemic redox state. *Redox Biol* **41**, 101881 (2021).
14. Bosma, M. *et al.* FNDC4 acts as an anti-inflammatory factor on macrophages and improves colitis in mice. *Nat. Commun.* **7**, 11314 (2016).
15. Sun, R., Xu, C., Feng, B., Gao, X. & Liu, Z. Critical roles of bile acids in regulating intestinal mucosal immune responses. *Therap. Adv. Gastroenterol.* **14**, 17562848211018098 (2021).
16. Zhou, X. *et al.* PPARα-UGT axis activation represses intestinal FXR-FGF15 feedback signalling and exacerbates experimental colitis. *Nat. Commun.* **5**, 4573 (2014).
17. Balic, J. J. *et al.* STAT3 serine phosphorylation is required for TLR4 metabolic reprogramming and IL-1β expression. *Nat. Commun.* **11**, 3816 (2020).
18. Sakai, J. *et al.* Lipopolysaccharide-induced NF-κB nuclear translocation is primarily dependent on MyD88, but TNFα expression requires TRIF and MyD88. *Sci. Rep.* **7**, 1428 (2017).
19. Zhou, Z., Xu, M.-J. & Gao, B. Hepatocytes: a key cell type for innate immunity. *Cell. Mol. Immunol.* **13**, 301–315 (2016).
20. Ahyi, A.-N. N. *et al.* Roles of STAT3 in protein secretion pathways during the acute-phase response. *Infect. Immun.* **81**, 1644–1653 (2013).
21. Hernández-Chirlaque, C. *et al.* Germ-free and Antibiotic-treated Mice are Highly Susceptible to Epithelial Injury in DSS Colitis. *J. Crohns. Colitis* **10**, 1324–1335 (2016).

22. Zarrinpar, A. *et al.* Antibiotic-induced microbiome depletion alters metabolic homeostasis by affecting gut signaling and colonic metabolism. *Nat. Commun.* **9**, 2872 (2018).
23. Chassaing, B., Aitken, J. D., Malleshappa, M. & Vijay-Kumar, M. Dextran sulfate sodium (DSS)-induced colitis in mice. *Curr. Protoc. Immunol.* **104**, 15.25.1–15.25.14 (2014).
24. Zhou, H. & Hylemon, P. B. Bile acids are nutrient signaling hormones. *Steroids* **86**, 62–68 (2014).
25. Bromke, M. A. & Krzystek-Korpacka, M. Bile Acid Signaling in Inflammatory Bowel Disease. *Int. J. Mol. Sci.* **22**, (2021).
26. Honda, A. *et al.* Regulation of bile acid metabolism in mouse models with hydrophobic bile acid composition. *J. Lipid Res.* **61**, 54–69 (2020).
27. Gong, Z. *et al.* Chenodeoxycholic acid activates NLRP3 inflammasome and contributes to cholestatic liver fibrosis. *Oncotarget* **7**, 83951–83963 (2016).
28. Horikawa, T. *et al.* Chenodeoxycholic Acid Releases Proinflammatory Cytokines from Small Intestinal Epithelial Cells Through the Farnesoid X Receptor. *Digestion* **100**, 286–294 (2019).
29. Ananthakrishnan, A. N. *et al.* Environmental triggers in IBD: a review of progress and evidence. *Nat. Rev. Gastroenterol. Hepatol.* **15**, 39–49 (2018).
30. de Souza, H. S. P. & Fiocchi, C. Immunopathogenesis of IBD: current state of the art. *Nat. Rev. Gastroenterol. Hepatol.* **13**, 13–27 (2016).
31. Gómez-Gómez, G. J., Masedo, Á., Yela, C., Martínez-Montiel, M. del P. & Casís, B. Current stage in inflammatory bowel disease: What is next? *World J. Gastroenterol.* **21**, 11282–11303 (2015).
32. Veloso, F. T. Extraintestinal manifestations of inflammatory bowel disease: do they influence treatment and outcome? *World J. Gastroenterol.* **17**, 2702–2707 (2011).
33. Kim, S. L., Shin, M. W. & Kim, S. W. Lipocalin 2 activates the NLRP3 inflammasome via LPS-induced NF-κB signaling and plays a role as a pro-inflammatory regulator in murine macrophages. *Mol. Med. Rep.* **26**, (2022).
34. Chawla, M. *et al.* An epithelial pathway exacerbates intestinal inflammation by supplementing

latent RelA dimers to the canonical NF-κB module. *Proc. Natl. Acad. Sci. U. S. A.* **118**, (2021).

35. Shi, Y., Liu, Z., Cui, X., Zhao, Q. & Liu, T. Intestinal vitamin D receptor knockout protects from oxazolone-induced colitis. *Cell Death Dis.* **11**, 461 (2020).
36. Weisser, S. B. *et al.* SHIP-deficient, alternatively activated macrophages protect mice during DSS-induced colitis. *J. Leukoc. Biol.* **90**, 483–492 (2011).
37. Bessman, N. J. *et al.* Dendritic cell-derived hepcidin sequesters iron from the microbiota to promote mucosal healing. *Science* **368**, 186–189 (2020).
38. Quinton, L. J. *et al.* Hepatocyte-specific mutation of both NF-κB RelA and STAT3 abrogates the acute phase response in mice. *J. Clin. Invest.* **122**, 1758–1763 (2012).
39. Hilliard, K. L. *et al.* The lung-liver axis: A requirement for maximal innate immunity and hepatoprotection during pneumonia. *Am. J. Respir. Cell Mol. Biol.* **53**, 378–390 (2015).
40. Sinha, S. R. *et al.* Dysbiosis-induced secondary bile acid deficiency promotes intestinal inflammation. *Cell Host Microbe* **27**, 659–670.e5 (2020).
41. Yang, M. *et al.* Bile Acid-Gut Microbiota Axis in Inflammatory Bowel Disease: From Bench to Bedside. *Nutrients* **13**, (2021).
42. Shalon, D. *et al.* Profiling the human intestinal environment under physiological conditions. *Nature* **617**, 581–591 (2023).
43. Gui, W. *et al.* Colitis ameliorates cholestatic liver disease via suppression of bile acid synthesis. *Nat. Commun.* **14**, 3304 (2023).
44. Chen, L. *et al.* Hepatic cytochrome P450 8B1 and cholic acid potentiate intestinal epithelial injury in colitis by suppressing intestinal stem cell renewal. *Cell Stem Cell* **29**, 1366–1381.e9 (2022).
45. Eloranta, J. J. & Kullak-Ublick, G. A. The Role of FXR in Disorders of Bile Acid Homeostasis. *Physiology* (2008) doi:10.1152/physiol.00020.2008.
46. Camilleri, M. & Gores, G. J. Therapeutic targeting of bile acids. *Am. J. Physiol. Gastrointest. Liver Physiol.* **309**, G209–15 (2015).

47. Paramsothy, S. *et al.* Specific Bacteria and Metabolites Associated With Response to Fecal Microbiota Transplantation in Patients With Ulcerative Colitis. *Gastroenterology* **156**, 1440–1454.e2 (2019).

48. Kiesler, P., Fuss, I. J. & Strober, W. Experimental Models of Inflammatory Bowel Diseases. *Cell Mol Gastroenterol Hepatol* **1**, 154–170 (2015).

49. Ward, J. B. J. *et al.* Ursodeoxycholic acid and lithocholic acid exert anti-inflammatory actions in the colon. *Am. J. Physiol. Gastrointest. Liver Physiol.* **312**, G550–G558 (2017).

50. Gaikwad, N. W. Bileome: The bile acid metabolome of rat. *Biochem. Biophys. Res. Commun.* **533**, 458–466 (2020).

Figure and Figure Legends

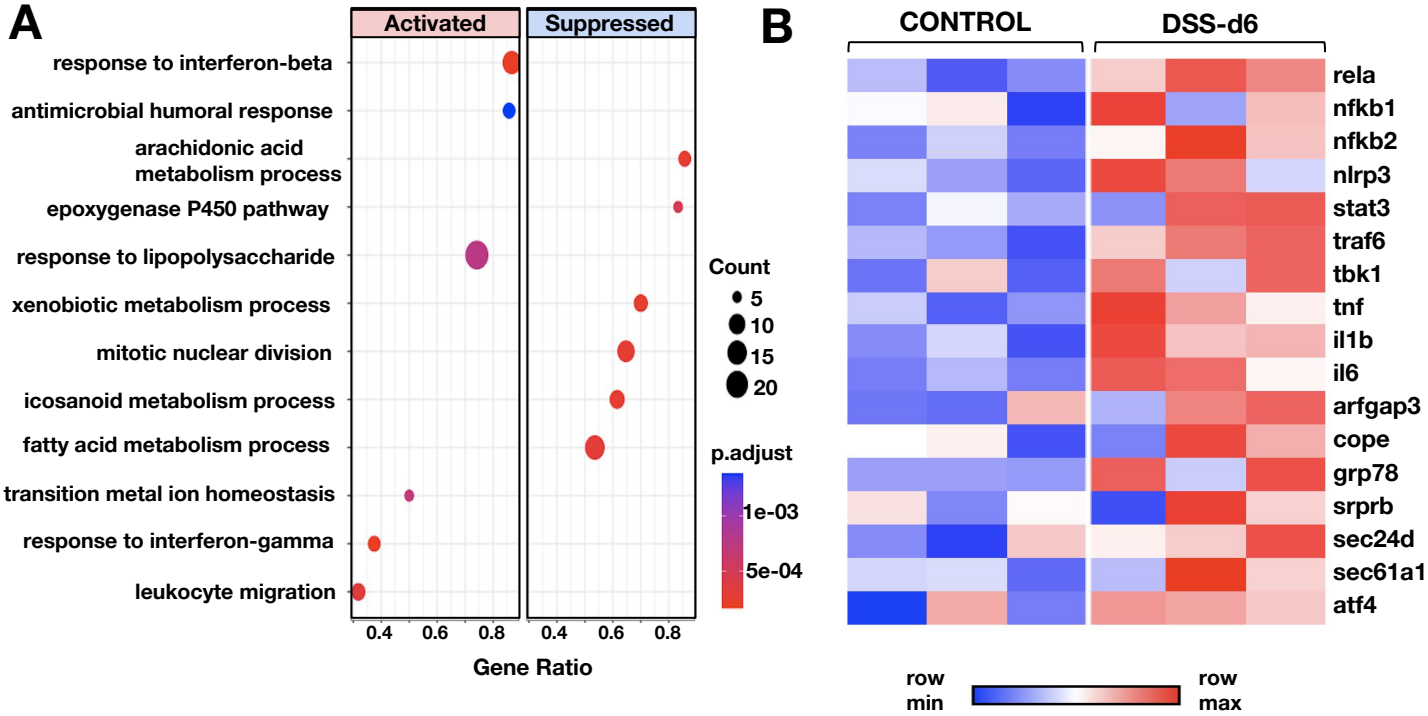

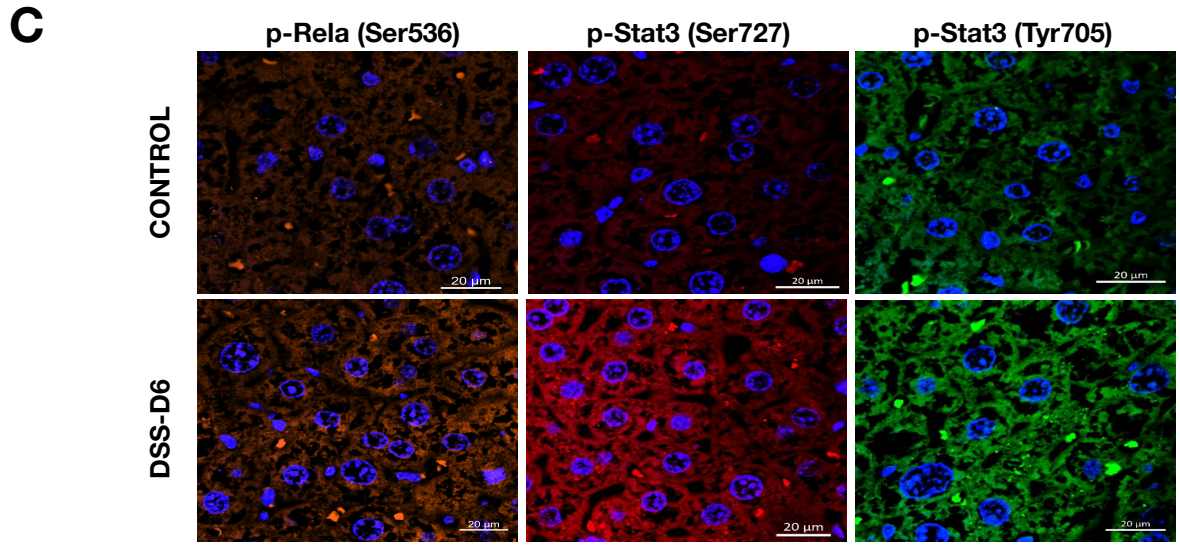

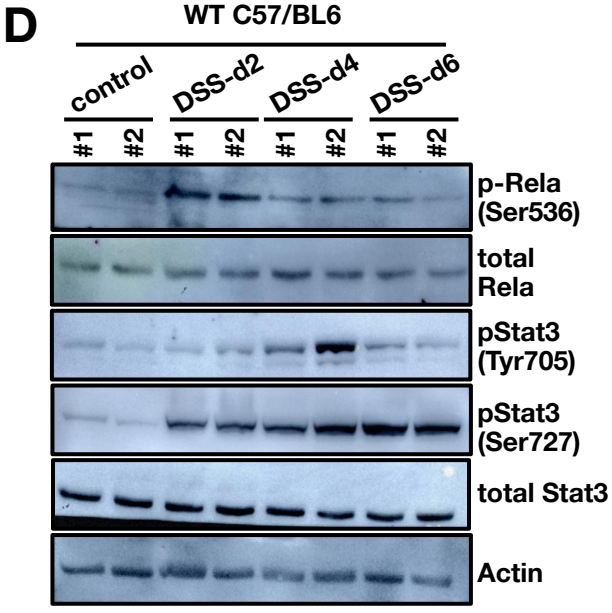

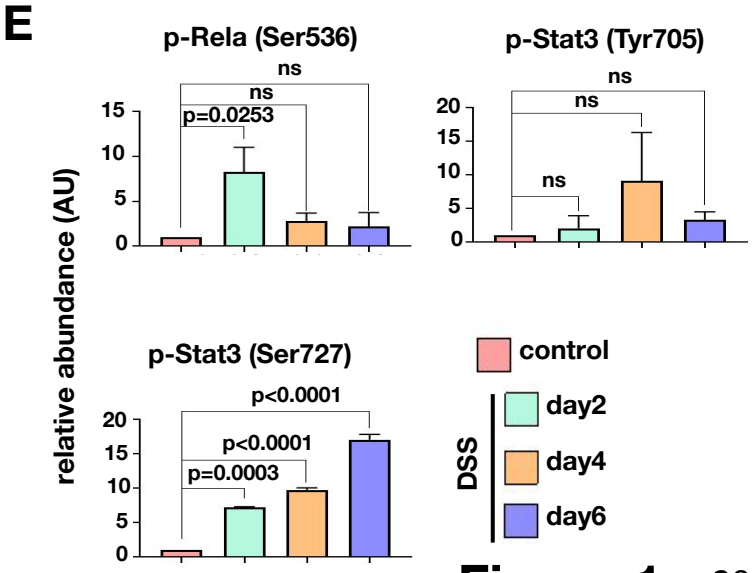

Figure 1

Figure 1: Initiation of colitis in mice leads to hepatic Rela and Stat3 activation. (A) GO pathway enrichment analysis was done for DEGs with adjusted p-value < 0.05 on days 6 post DSS treatment. Bubble plot depicts the enrichment of pathways on day 6 for different genotypes, where the coordinate on x-axis represents gene ratio, size of bubble represents the gene count and colour represents the p-value. **(B)** Heatmap represents normalized transcript count of the Rela and Stat3 pathway obtained from the RNA-seq experiment of three biological replicates. Scale is normalized across each row and colour from blue to red represents minimum and the maximum values respectively. **(C)** Representative confocal microscopy images show Rela and Stat3 activation in untreated and 6 days DSS-treated liver tissue of C57BL/6 mice. Images were taken at 40X. Scale is 20 μm. **(D)** Western blot revealing the abundance of total Rela and total Stat3, and their phosphorylated functionally active forms, in the liver extracts prepared from wild type C57BL/6 mice either left untreated or subjected to DSS treatment for two, four and six days respectively. **(E)** The signal intensity of bands corresponding to the indicated phosphorylated proteins was quantified from western blots, normalized against beta-actin, and presented as a bar plot. The data represent the means of three biological replicates ± SEM.

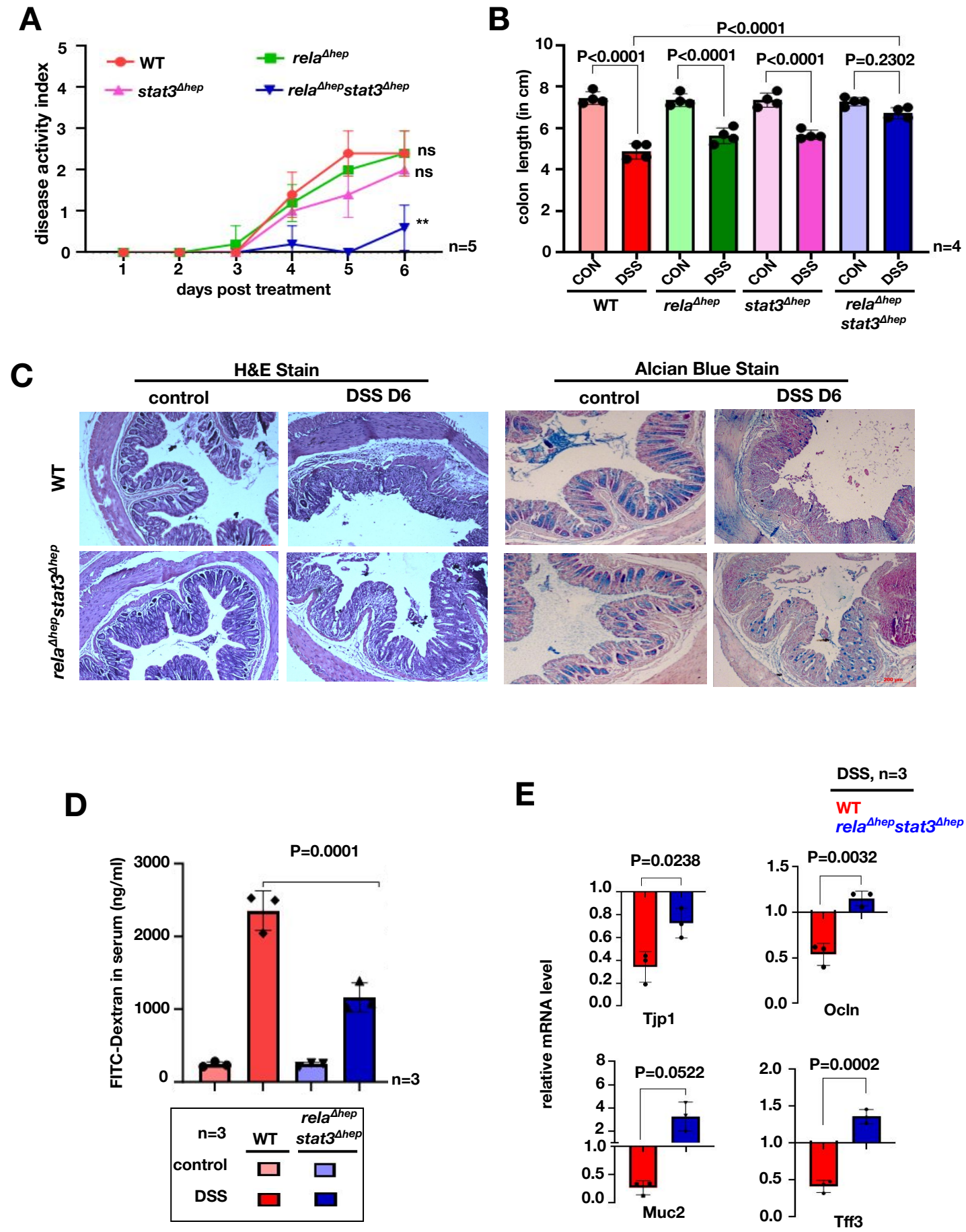
A
disease activity index
WT
stat3Δhep
relaΔhep
relaΔhepstat3Δhep
ns
ns
**
n=5
days post treatment
B
colon length (in cm)
P<0.0001
P<0.0001
P<0.0001
P<0.0001
P=0.2302
n=4
CON
DSS
WT
relaΔhep
stat3Δhep
relaΔhep stat3Δhep
C
H&E Stain
Alcian Blue Stain
control
DSS D6
WT
relaΔhepstat3Δhep
D
FITC-Dextran in serum (ng/ml)
P=0.0001
n=3
n=3
WT
relaΔhep stat3Δhep
control
DSS
E
DSS, n=3
WT
relaΔhepstat3Δhep
relative mRNA level
P=0.0238
Tjp1
P=0.0032
Ocln
P=0.0522
Muc2
P=0.0002
Tff3

Figure 2

Figure 2: ***rela* and *stat3* deficiency in hepatocytes ameliorates DSS-induced acute colitis in mice. (A)** Line plot charting disease activity index of wild type, *rela*$^{\Delta hep}$, *stat3*$^{\Delta hep}$ and *rela*$^{\Delta hep}$*stat3*$^{\Delta hep}$ littermate mice subjected to treatment with 2% DSS for six days. **(B)** Bar plot depicting colon length measured on day six post-onset of DSS treatment of mice of the indicated genotypes. Untreated wild type littermates of corresponding genotypes were used as controls. **(C)** Colon sections from untreated and DSS-treated mice of the indicated genotypes were examined for histological features involving H&E staining [left panel] and alcian blue staining [right panel]. Data were obtained in 10X magnification and represent three experimental replicates; two fields per section and a total of three sections from each set were examined. **(D)** Bar plot quantifying gut permeability of untreated and DSS-treated wild type and *rela*$^{\Delta hep}$*stat3*$^{\Delta hep}$ mice. Briefly, the serum concentration of FITC was measured six hours after oral gavaging the mice with FITC-dextran. **(E)** RT-qPCR revealing the relative abundance of the indicated mRNAs encoding broadly enterocyte-specific (above panel) or goblet cell-specific (below panel) markers in untreated or DSS-treated mice of the indicated genotypes.

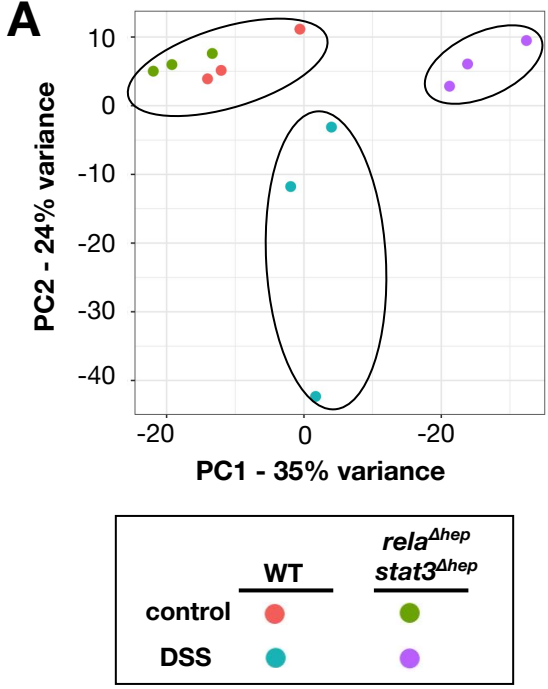
A
PC2 - 24% variance
PC1 - 35% variance
10
0
-10
-20
-30
-40
-20
0
-20
WT
rela$^{\Delta hep}$ stat3$^{\Delta hep}$
control
DSS

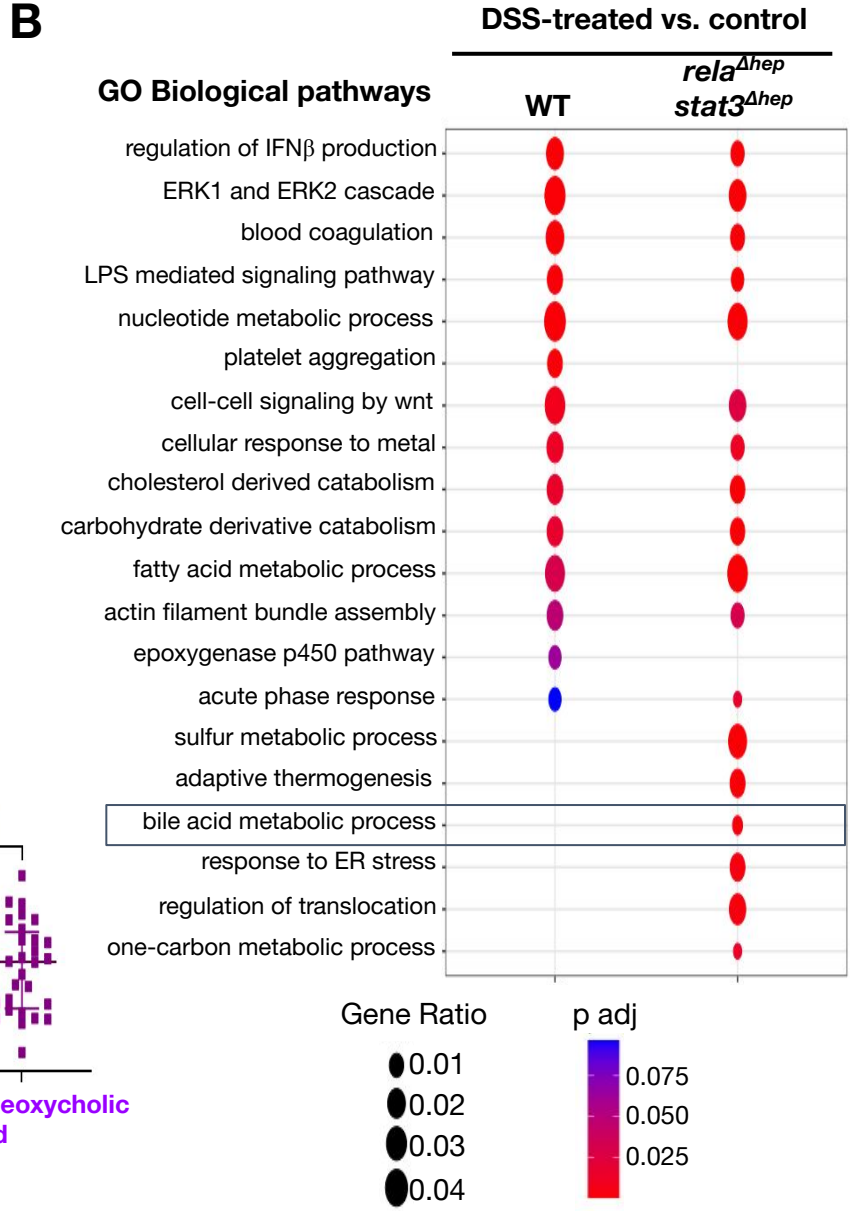
B
DSS-treated vs. control
GO Biological pathways
WT
rela$^{\Delta hep}$ stat3$^{\Delta hep}$
regulation of IFNβ production
ERK1 and ERK2 cascade
blood coagulation
LPS mediated signaling pathway
nucleotide metabolic process
platelet aggregation
cell-cell signaling by wnt
cellular response to metal
cholesterol derived catabolism
carbohydrate derivative catabolism
fatty acid metabolic process
actin filament bundle assembly
epoxygenase p450 pathway
acute phase response
sulfur metabolic process
adaptive thermogenesis
bile acid metabolic process
response to ER stress
regulation of translocation
one-carbon metabolic process
Gene Ratio
0.01
0.02
0.03
0.04
p adj
0.075
0.050
0.025

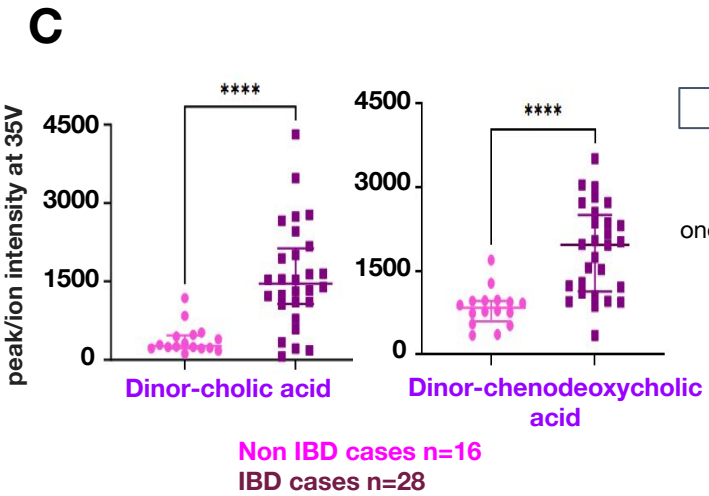
C
peak/ion intensity at 35V
4500
3000
1500
0
****
Dinor-cholic acid
Dinor-chenodeoxycholic acid
Non IBD cases n=16
IBD cases n=28

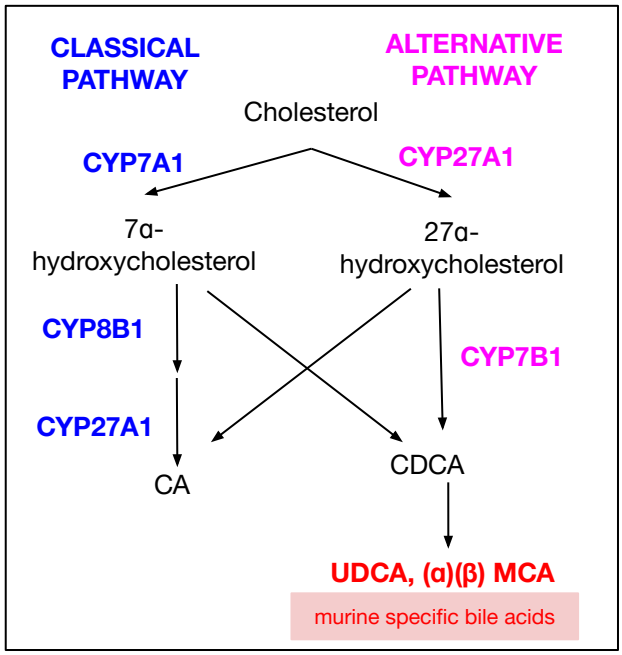
D
CLASSICAL PATHWAY
ALTERNATIVE PATHWAY
Cholesterol
CYP7A1
CYP27A1
7α-hydroxycholesterol
27α-hydroxycholesterol
CYP8B1
CYP7B1
CYP27A1
CA
CDCA
UDCA, (α)(β) MCA
murine specific bile acids

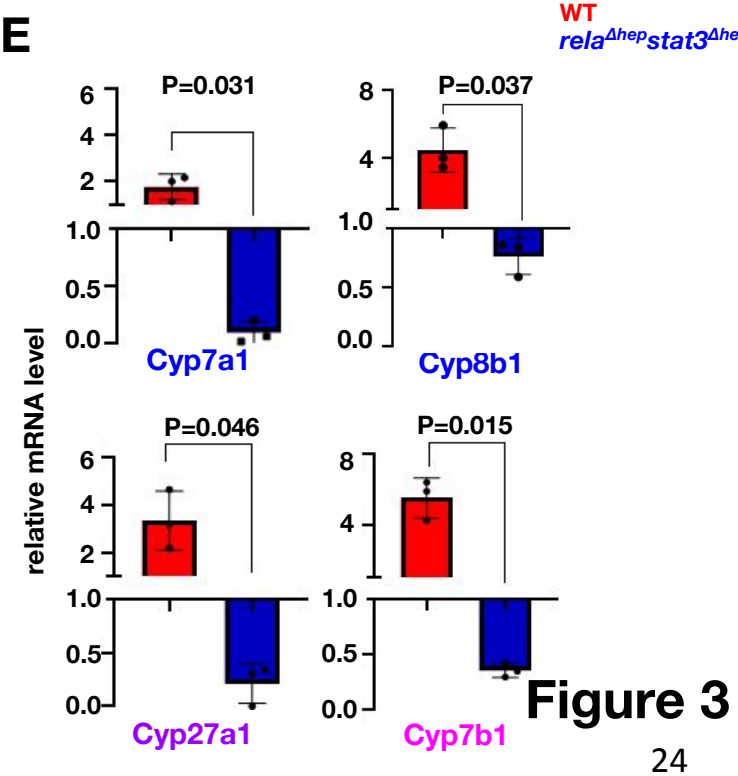
E
DSS, n=3
WT
rela$^{\Delta hep}$stat3$^{\Delta he}$
relative mRNA level
P=0.031
Cyp7a1
P=0.037
Cyp8b1
P=0.046
Cyp27a1
P=0.015
Cyp7b1

Figure 3

Figure 3: **Charting hepatic gene expressions in colitogenic wild type and *rela*$^{\Delta hep}$*stat3*$^{\Delta hep}$ mice. (A)** PCA plot illustrating the hepatic transcriptome, identified through global RNA-seq analyses, of untreated or DSS-treated wild type and *rela*$^{\Delta hep}$*stat3*$^{\Delta hep}$ mice (n=3). DSS treatment was carried out for six days. **(B)** Bubble plot depicting the relative enrichment of GO biological terms for differentially expressed genes in wild type or *rela*$^{\Delta hep}$*stat3*$^{\Delta hep}$ mice. The gene ratio for a given term and the adjusted p value associated with the enrichment score has been presented for the individual genetic backgrounds. **(C)** Dot plot of dinor-cholic acid and dinor-chenodeoxycholic acid as detected in an untargeted LC-MS based quantification of bile acids in the mucosal biopsy samples from IBD and Non-IBD patients. **(D)** Schematic presentation of classical and alternate pathways of bile synthesis in mice liver tissue. CA, CDCA, MCA and UDCA represent cholic, chenodeoxycholic, muricholic and ursodeoxycholic acids, respectively. **(E)** RT-qPCR analyses comparing the hepatic abundance of indicated mRNAs encoding enzymes involved in bile metabolism in DSS-treated wild type and *rela*$^{\Delta hep}$*stat3*$^{\Delta hep}$ mice (n=3). Fold change is relative to their corresponding wild type littermates.

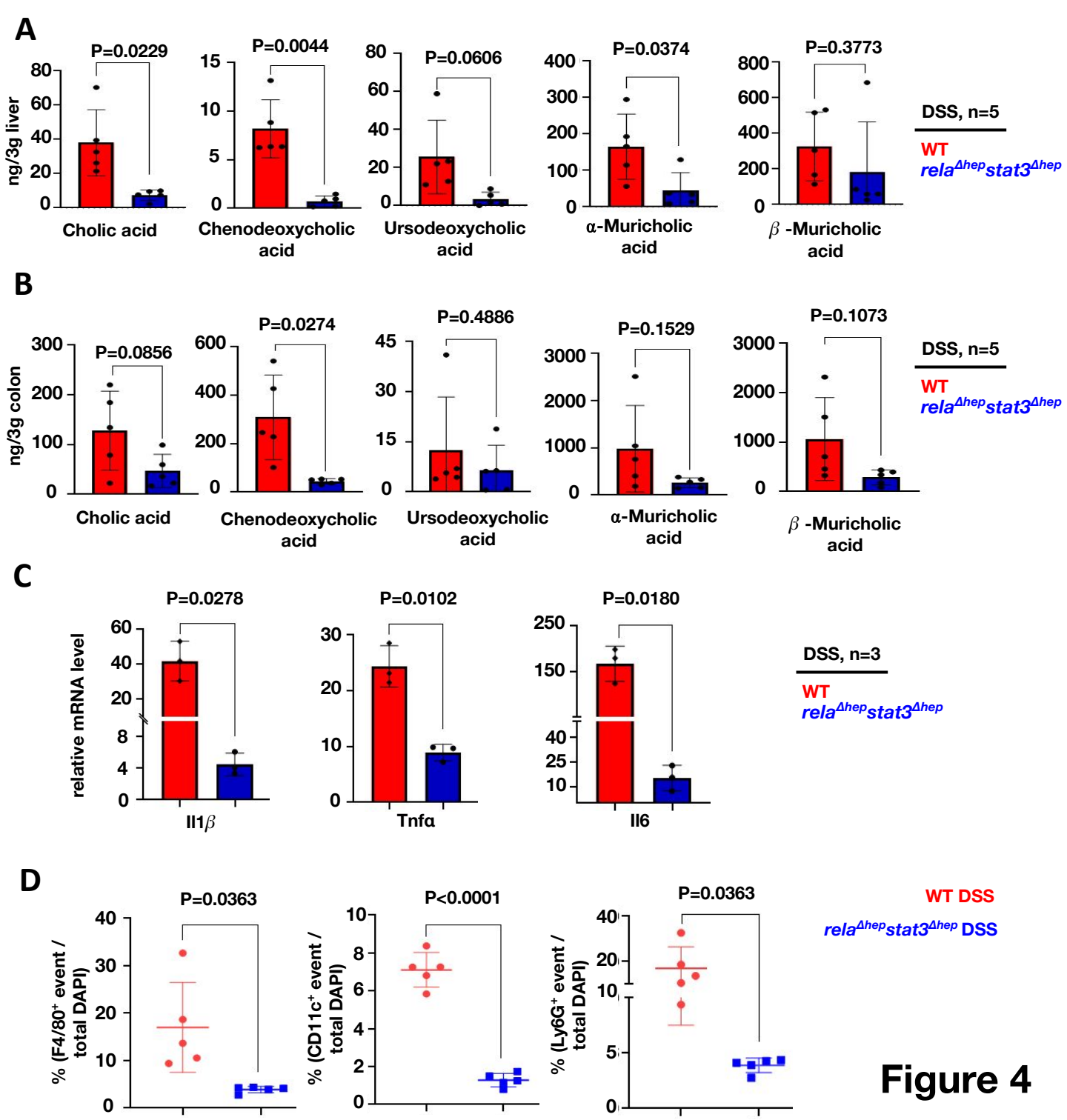

Figure 4: Altered accumulation of primary bile acids in *rela*$^{\Delta hep}$*stat3*$^{\Delta hep}$ mice accompanies a less severe inflammatory signature in the colitogenic gut. Targeted LC-MS based quantification of primary bile acid in the liver **(A)** and the colon **(B)** of DSS-treated wild type and *rela*$^{\Delta hep}$*stat3*$^{\Delta hep}$ mice (n=5). **(C)** RT-qPCR analyses comparing the colonic abundance of indicated mRNAs encoding pro-inflammatory cytokines (n=3) for DSS-treated wild type and *rela*$^{\Delta hep}$*stat3*$^{\Delta hep}$ mice. Fold change is relative to their corresponding wild type littermates. **(D)** Dot-plot representing the frequency of F4/80$^+$, CD11c$^+$ and Ly6G$^+$ cells among total DAPI-stained cells in the colon sections derived from DSS-treated wild type and *rela*$^{\Delta hep}$*stat3*$^{\Delta hep}$ mice.

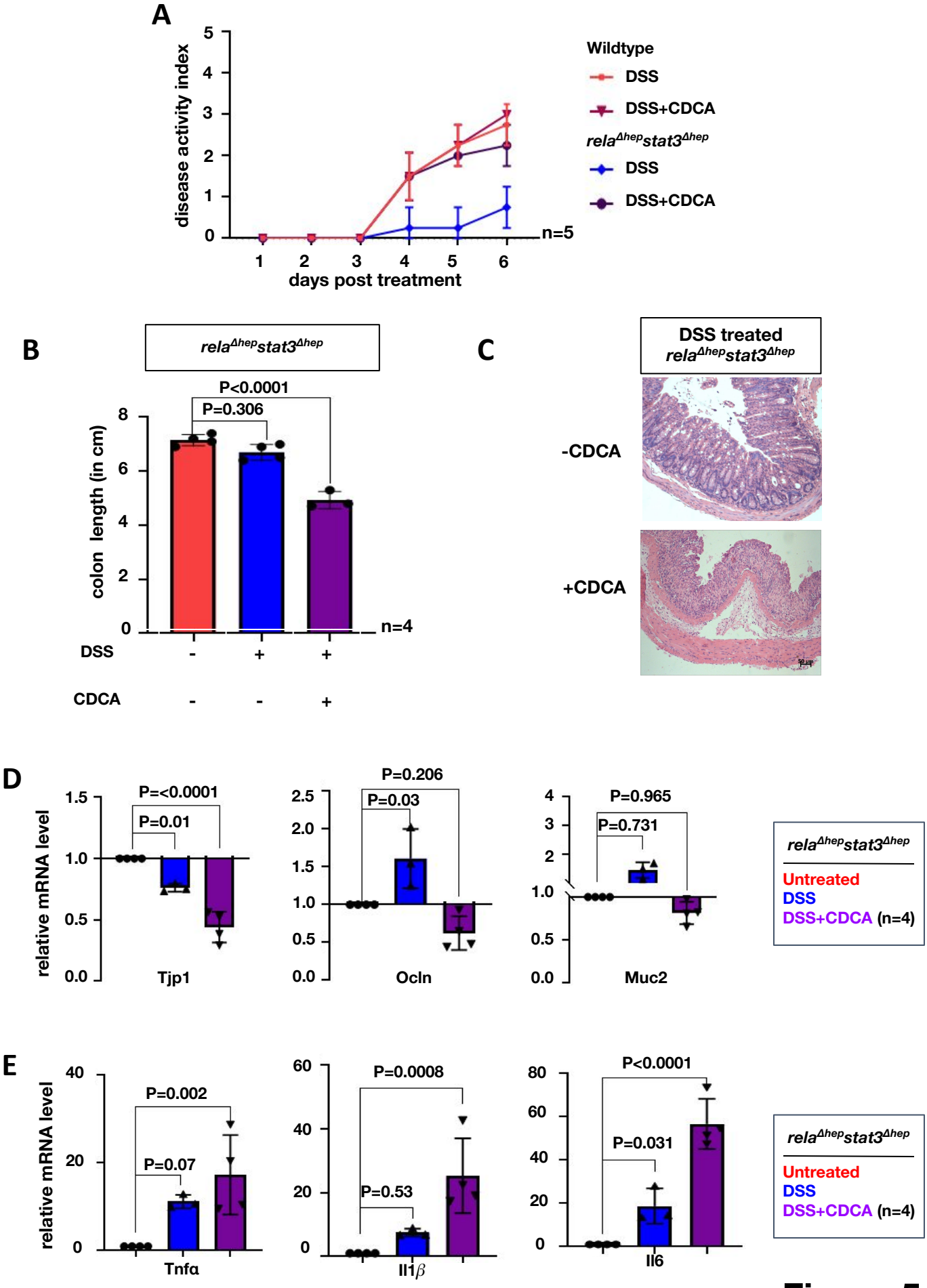
A
disease activity index
days post treatment
n=5
Wildtype
DSS
DSS+CDCA
rela^Δhep stat3^Δhep
DSS
DSS+CDCA
B
rela^Δhep stat3^Δhep
colon length (in cm)
P<0.0001
P=0.306
n=4
DSS
CDCA
C
DSS treated
rela^Δhep stat3^Δhep
-CDCA
+CDCA
D
relative mRNA level
P=<0.0001
P=0.01
Tjp1
P=0.206
P=0.03
Ocln
P=0.965
P=0.731
Muc2
rela^Δhep stat3^Δhep
Untreated
DSS
DSS+CDCA (n=4)
E
relative mRNA level
P=0.002
P=0.07
Tnfα
P=0.0008
P=0.53
Il1β
P<0.0001
P=0.031
Il6
rela^Δhep stat3^Δhep
Untreated
DSS
DSS+CDCA (n=4)

Figure 5

Figure 5: Supplementing chenodeoxycholic acid (CDCA) restores the colitogenic sensitivity in *rela*$^{\Delta hep}$*stat3*$^{\Delta hep}$ mice. (A) Line plot charting the disease activity in a time course of wild type and *rela*$^{\Delta hep}$*stat3*$^{\Delta hep}$ mice subjected to DSS treatment while being supplemented with 10 mg/kg CDCA daily. Mice devoid of CDCA supplementation were treated with DMSO as controls. **(B)** Bar plot comparing the colon length of *rela*$^{\Delta hep}$*stat3*$^{\Delta hep}$ mice subjected to DSS treatment for six days in the absence or presence of CDCA supplementation. **(C)** H&E stained colon sections from DSS-treated *rela*$^{\Delta hep}$*stat3*$^{\Delta hep}$ mice with and without CDCA supplementation. Data were obtained in 10X magnification, this is a representative of three experimental replicates and a total of four sections from each set were examined. RT-qPCR analyses comparing the colonic abundance of indicated mRNAs encoding **(D)** IEC-specific markers and **(E)** pro-inflammatory cytokines in mice subjected to DSS treatment for six days in the absence or presence of CDCA supplementation (n=4). Untreated *rela*$^{\Delta hep}$*stat3*$^{\Delta hep}$ mice were used as controls.

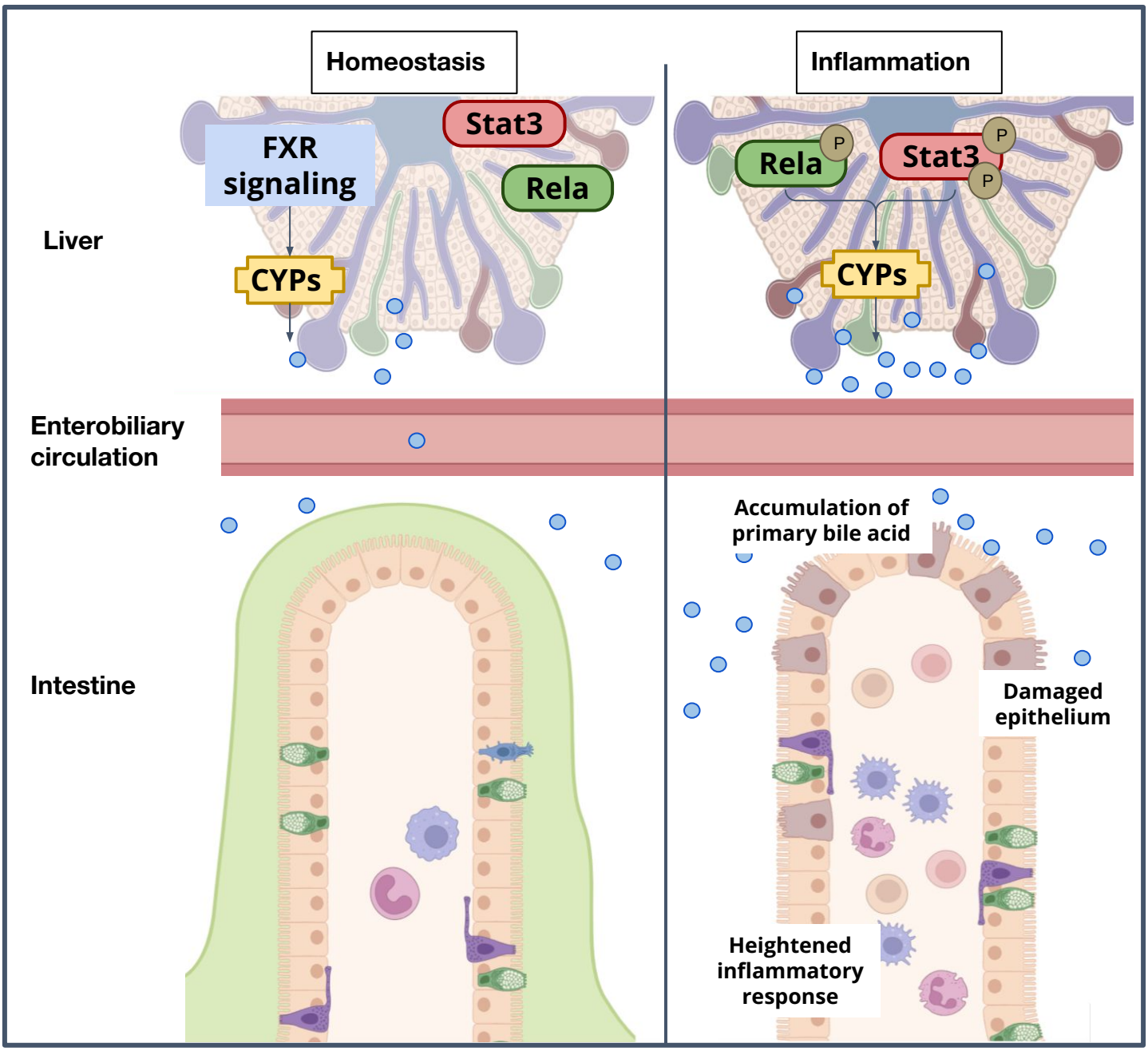

Figure 6

Figure 6: A model depicting the immuno-metabolic network linking the inflammation induced hepatic signaling pathway to intestinal pathologies in mice.